PAPER

Anticancer activity of a chelating nitrogen mustard bearing tetrachloridoplatinum(IV) complex: better stability yet equipotent to the Pt(II) analogue†

Subhendu Karmakar, Saptarshi Chatterjee, Kallol Purkait and Arindam Mukherjee*

Two Pt(IV) complexes *cis,cis,trans*-[Pt^IV(L1)Cl$_4$] (**1a**) & *cis,cis,trans*-[Pt^IV(L2)Cl$_4$] (**2a**) containing the nitrogen mustard moieties $-N(CH_2CH_2Cl)_2$ & $-NHCH_2CH_2Cl$, were prepared in a single step from the Pt(II) complexes containing $-N(CH_2CH_2OH)_2$ (**1**) & $-NHCH_2CH_2OH$ (**2**) moieties respectively using only thionyl chloride. The characterization of both the Pt(IV) complexes was performed by NMR, IR, UV and elemental analysis. Complex **1a** was also characterized by single crystal X-ray diffraction. **1a** crystallized in the *I2/a* space group. **1a** exhibited much higher solution stability than **2a** in kinetic studies by ^{1}H NMR. **1a** shows a prodrug like activity as it converts to its Pt(II) congener, [Pt^II(L1)Cl$_2$] (**3**) after 2 days in buffered solution. The binding experiment of **1a** with model nucleobase 9-ethylguanine (9-EtG), showed that **1a** converts to **3** and forms mono-adducts with 9-EtG. In the presence of reduced glutathione (GSH), the formation of **3** from **1a** is quicker and upon the formation of **3** it binds almost instantaneously to GSH to form *cis*-[PtCl(L1)SG] (**3c**). Complex **3c** transformed within a day to give a free aziridinium ion of L1 (**3b**) by dissociation. The *in vitro* cytotoxicity of the complexes and the clinical anticancer drug cisplatin show that **1a** is potent against MCF-7, A549, HepG2 and MIA PaCa-2. The potency is highest against MIA PaCa-2 exhibiting an IC$_{50}$ value of 4.4 ± 0.5 µM. The *in vitro* cytotoxicity data also showed that between the two complexes only **1a** is active against MCF-7, A549 and MIA PaCa-2 in normoxia and hypoxia, both in the presence and absence of added GSH. Even in the presence of excess GSH in hypoxia, **1a** exhibits significant cytotoxicity against MIA PaCa-2 and MCF-7 with IC$_{50}$ values of 4.5 ± 0.3 and 11.2 ± 1.8 µM respectively. Platinum accumulation studies by ICP-MS display greater internalization of **1a**, than **2a**, **3** and cisplatin inside MCF-7 cells. **1a** arrests cell cycle at the G2/M phase in MCF-7, exhibits capability to inhibit metastasis, induces apoptotic cell death and displays blood compatibility with human blood.

Introduction

The serendipitous discovery of cisplatin by Barnett Rosenberg and his co-workers was the landmark in the use of metal complexes as chemotherapeutic agents.[1–3] Despite having several limitations,[4] a great clinical success was achieved in using cisplatin for the treatment of various types of cancer.[5–7] The limitations of the usage of cisplatin mainly lie in the area of severe toxicities leading to major side-effects[8–11] and tumor resistance to drugs.[12–14] In order to counter the limitations, drugs like oxaliplatin and carboplatin have emerged and are serving

Department of Chemical Sciences, Indian Institute of Science Education and Research Kolkata, Mohanpur-741246, India. E-mail: a.mukherjee@iiserkol.ac.in

†Electronic supplementary information (ESI) available: Additional crystallographic data, NMR data of synthesized compounds, NMR & ESI-MS data of stability and binding kinetics, tables containing ESI-MS speciation, isotope modelling of ESI-MS speciation, plots of MTT assay, cell cycle arrest histograms, fluorescence microscopy image, data of hemolysis assay, detailed experimental procedures. CCDC 1449897. For ESI and crystallographic data in CIF or other electronic format see DOI: 10.1039/c6dt00831c

well in clinic for the treatment of various types of cancer.[15,16] All the above drugs are square planar Pt(II) complexes. It has been found that after systematic hydrolysis at the metal centre, the drug generates labile sites which cross-link the DNA bases, followed by a cascade that triggers cell death.[17,18] However, square planar Pt(II) complexes are known to start early hydrolysis *i.e.* before even reaching the target, a significant amount of a Pt(II) drug is hydrolyzed and reacts with various ingredients of blood plasma and several intra- and extracellular biomolecules to generate unwanted toxicities. Since there is a loss of the drug the effective applied dosage becomes low, requiring more drug to be given for the desired effect. It is found that on oxidation of Pt(II) to Pt(IV), the resulting d^6 electronic configuration stabilizes the octahedral geometry and reduces reactivity. Hence, a Pt(IV) complex may possess enough kinetic inertness to resist immature hydrolysis and other unwanted side reactions with bio-molecules.[19,20]

The cytotoxicity of the Pt(IV) complexes is known to arise due to their reduction to Pt(II) in the cellular reducing environment, especially in the hypoxic tumor environment where bio-

Scheme 1 Bioreduction of Pt(IV) complexes in the presence of reducing bio-molecules.

Scheme 2 Synthetic methods for the preparation of Pt(IV) complexes (**1a** & **2a**) and the structure of the Pt(II) counterpart of **1a** (**3**).

molecules *viz.* glutathione and ascorbic acid act as reducing agents (Scheme 1).[19,21–23] Such a pro-drug like activity is one of the added advantages in designing Pt(IV) complexes over Pt(II) drugs.[24–26] Out of the numerous Pt(IV) complexes designed so far, four Pt(IV) complexes were subjected to clinical trials (Chart 1A),[26,27] but iproplatin was abandoned from clinical trials due to less reactivity compared to cisplatin (or carboplatin) and tetraplatin was abandoned due to its severe neurotoxicity.[15,26,28,29] Amongst all four the orally active satraplatin showed promising clinical activity in combination therapy as well as a standalone drug against various cancers especially against prostate cancer and is still in clinical trials.[15,26,28,29] LA-12 is a very similar analogue of satraplatin, whose clinical trial is ongoing (phase I & II, yet unpublished).[26,29,30] Therefore, designing a suitable Pt(IV) anticancer agent still remains a challenge.

In a Pt(IV) complex the axial ligands are lost during the time of reduction to Pt(II). The presence of the axial ligands would influence the redox potentials of a Pt(IV) complex even if the equatorial ligands are the same in two different complexes. Among the numerous axial ligands used, some popular axial ligands with decreasing order of reducing ability of the Pt(IV) complex may be represented as $-OCOCF_3 > -Cl > -OCOCH_3 > -OH$.[31] In this work we have chosen $-Cl$ as the axial ligand

with the thought that it would render an intermediate redox potential to the designed Pt(IV) complex. In our ligand design we have used the pyridine containing nitrogen mustard (L1) which gave us valuable information during our work on the Pt(II) complex (**3**, Scheme 2).[32] We have synthesized the Pt(IV) mustard complex **1a** in a single step from the Pt(II) complex of the ligand bis(2-hydroxyethyl)-pyridylmethylamine with $SOCl_2$ in good yield (Scheme 2). For the sake of comparison of activity we also synthesized a Pt(IV) complex (**2a**) bearing a $-NHCH_2CH_2Cl$ group in the ligand (L2) instead of the mustard group, $-N(CH_2CH_2Cl)_2$ (Scheme 2).

Complex **1a** has a chelating mustard ligand at the equatorial position along with two equatorial and two axial $-Cl^-$ ions. The alkylating ability of the nitrogen mustards is well known and they have a rich history in chemotherapy (Chart 1B) against various forms of cancers.[33] They form an inter-strand crosslink with N^7 of guanine in DNA upon generation of the aziridinium ion as an intermediate.[34,35] It is known that the reactivity of nitrogen mustards can be tuned by controlling the availability/reactivity of the lone pair of nitrogen on the mustard moiety, $-N(CH_2CH_2Cl)_2$. The donation of the nitrogen lone pair to the metal centre, during the formation of complexes reduces the reactivity of the nitrogen mustard to form the aziridinium ion, thus controlling the alkylating ability. The metal bound mustard group would be reactivated upon the loss of a metal ion due to the higher availability of the lone pair on the nitrogen of the mustard group.[36–43] However, in spite of this knowledge only three Pt(IV) complexes are reported so far, *cis,cis,trans*-[Pt^{IV}XYCl$_4$],[44] *cis,cis,trans*-[Pt^{IV}X$_2$Cl$_4$][45] and *trans,cis,cis*-[Pt^{IV}X$_2$Cl$_4$][45] (where X = bis(2-chloroethyl)amine & Y = aziridine). None of them is a chelating nitrogen mustard and none of them has been probed for anticancer activity either.

Our impetus for this work came from our success with Pt(II) complex **3** of the chelating nitrogen mustard ligand.[32] We were eager to know the influence of the nitrogen mustard on the reactivity of Pt(IV) complexes. This encouraged us to synthesize and characterize two Pt(IV) complexes with the molecular formula *cis,cis,trans*-[Pt^{IV}(L1)Cl$_4$] (**1a**) and *cis,cis,trans*-[Pt^{IV}(L2) Cl$_4$] (**2a**) and probe their potential as anticancer agents.
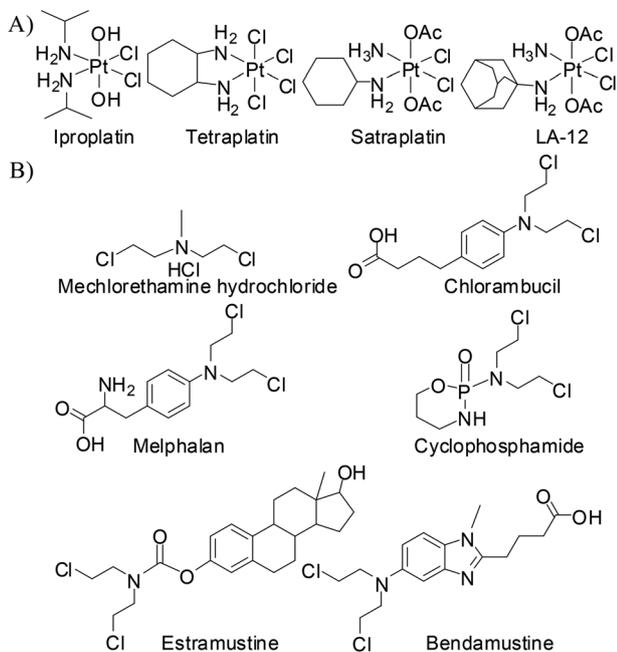
Chart 1 (A) Pt(IV) complexes in clinical trials and (B) nitrogen mustards in clinical use.

Results & discussion

Synthesis and characterization

Preparation of the Pt(IV) complex from Pt(II) precursors needs oxidation of the Pt(II) centre. The traditional method for oxidation of the Pt(II) centre is the use of an oxidizing agent like H_2O_2 in aqueous medium resulting in the formation of *trans*-dihydroxido Pt(IV). Further reactions are performed depending on which axial ligands are needed for derivatization, these include chlorination by purging Cl_2 gas, reaction with acid anhydrides, coupling reaction with any carboxylic acid derivative.[46] We have used $SOCl_2$ for the preparation of our *trans*-dichlorido Pt(IV) complexes. Both **1** & **2** were converted to **1a** & **2a** respectively within 8 h using neat $SOCl_2$ in a single step (Scheme 2). Here two different reactions concurred

$$[Pt^{II}Cl_2] + SOCl_2 \rightarrow [Pt^{IV}Cl_4] + [SO] \qquad (1)$$

$$2[SO] \rightarrow S + SO_2 \qquad (2)$$

in a single step; (i) oxidative addition of chlorine to the Pt(II) centre (eqn (1)) and (ii) substitution of the ligand's –OH group of **1** & **2** by the –Cl group to form **1a** & **2a** respectively with high yield (more than 90%). The byproduct of this reaction is SO_2 gas and elemental sulphur (eqn (2)). Sulphur was removed by washing several times with dry toluene and DCM. A similar process was reported in the literature in the presence of PCl_5 where both the oxidative chlorination of the Pt(II) centre and substitution of the ligand's –OH group by the –Cl group took place at the same time.[47] In our process the advantage is that the reaction time is less, there is no need of any solvent addition for performing the reaction and the isolation method of the desired complex is simple. In this context it would be worth mentioning that although $SOCl_2$ is known to oxidize various other metal centers by oxidative chlorination,[48–53] our reaction is the first report of the use of $SOCl_2$ for oxidative chlorination of the platinum centre. The sole relevant report in this regard is of a Pt(II) complex, where in the presence of $SOCl_2$ the ligand's –OH group converted to the –Cl group. However, there was no report of oxidation of the Pt(II) complex.[54]

Both the synthesized complexes (**1a** & **2a**) were characterized by multinuclear NMR techniques (^{1}H, ^{13}C & ^{195}Pt NMR), FT-IR and UV–vis spectroscopy. The IR spectra clearly showed the C–Cl stretching for **1a** & **2a** at 768 & 770 cm^{-1} respectively indicating –Cl functionalization by the nucleophilic substitution of $SOCl_2$ with the –OH group (Fig. S1†). The NMR data show that the shift of ^{1}H peaks supports the formation of Pt(IV) which differs from its reduced counterpart (**3**). The aromatic region of **3** contains four types of pyridine ring hydrogen. They are numbered as H3, H4, H5 & H6 and they appear in the NMR accordingly from a lower to higher field as H6, H4, H3 & H5 respectively. Upon oxidation of the platinum from +2 to +4 except for H6 and H10 (–CH_2Cl) all the other protons show a downfield shift by around 0.2–0.5 ppm. Such trends of the chemical shift are also found in the literature.[55,56] Apart from changes in the chemical shift, ^{195}Pt satellites were

observed in H6 & H7 (PyCH_2–) protons for **1a** which are absent in **3** and the coupling constant values ($^3J_{H–Pt}$) were 26.3 & 17.5 Hz respectively (Fig. S2†). In the case of **2a** also the ^{195}Pt satellites were found for H6 and one of the two H7 protons where the $^3J_{H–Pt}$ values are 26.3 and 18.7 Hz respectively (Fig. S7†). The ^{195}Pt chemical shift values −64.1 & −174.0 ppm for **1a** (Fig. S6†) & **2a** (Fig. S11†), respectively, were also in accordance with the +4 oxidation sate of platinum. The analytical purity of complexes was confirmed by CHN analysis which matches well with the calculated percentage of elements.

X-ray crystallography

A suitable single crystal of complex **1a** was obtained from an acetonitrile (acidified with HCl)–diethyl ether layer. **1a** crystallized in the monoclinic crystal system with the space group $I2/a$ (Table S1†). Each unit cell contains 8 complexes. The bond lengths of the two axial chlorides are higher than the equatorial two and the bond distance for Pt–N of the pyridine moiety is shorter than Pt–N of mustard nitrogen (Table S2†). The two axial chlorides are not exactly opposite to each other with respect to the Pt centre; rather they make a Cl–Pt–Cl angle of 175.84°. The structure shows that the two –CH_2CH_2Cl groups are projected above and below the coordination plane containing Pt, two N and two equatorial Cl^- (Fig. 1). The presence of four Cl^- coordinated to the Pt centre and the absence of any other cation in the lattice supports Pt in the oxidation state +4.

Compound stability in solution

The kinetic inertness of octahedral Pt(IV) complexes is well studied.[19,57] It is also known that all the complexes of Pt(IV) are not inert.[19] The inert nature depends strongly on the type of the axial ligand.[31] We have determined the solution stability of the Pt(IV) complex **1a** in 20% PBS (pD 7.4, prepared in D_2O) in DMSO-d_6 by ^{1}H NMR. The NMR data show that **1a** has excellent stability in buffered medium up to 1 d and only the original complex is visible in the NMR plots (Fig. 2). Hence, the kinetic inertness of **1a** towards hydrolysis is better than **3**,
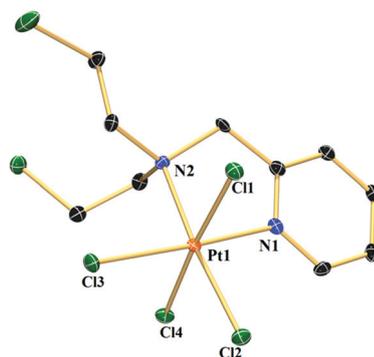
Fig. 1 ORTEP diagram of complex **1a**. Thermal ellipsoids are drawn at the 50% probability level. Hydrogen atoms are omitted for clarity. Selected bond lengths (Å): Pt1–Cl1 2.3286(7), Pt1–Cl4 2.3183(7), Pt1–Cl2 2.3165(7), Pt1–Cl3 2.3178(7), Pt1–N1 2.027(2) & Pt1–N2 2.155(2); selected bond angles (°): Cl4–Pt1–Cl1 175.84(3), Cl2–Pt1–Cl3 88.66(3) & N2–Pt1–N1 80.60(10).
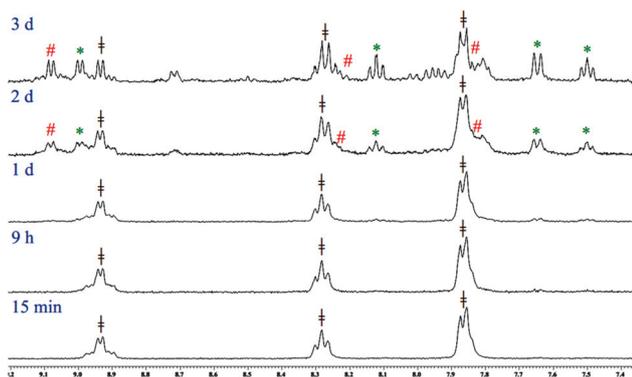
Fig. 2 Stack plot of the stability kinetic study of **1a** monitored by ^{1}H NMR at different time intervals in 20% PBS (pD 7.4, prepared in D$_2$O) – DMSO-d_6 mixture, where ‡ & * indicate unreacted complexes **1a** & **3** and # indicates hydrolyzed complex **3** (**3a**).

Scheme 3 Proposed reaction pathways of **1a** for the hydrolysis and binding of 9-EtG/GSH. The dotted arrow in the scheme depicts that the formation of **3b** from **3a** shows no distinct evidence.

which as per our earlier work, started to hydrolyze within 20 minutes. The additional kinetic stability should be helpful for **1a** to increase its circulation lifetime and entry into the cells. **1a** started to hydrolyze after 2 d and new peaks appeared at 9.08 & 9.00 (H6), 8.24 & 8.13 (H4), 7.84 & 7.65 (H3) and 7.51 (H5) ppm (see Scheme 2 for numbering; only the aromatic region of **1a** is shown for clarity). Among the three pairs of new peaks, the peaks at 9.00, 8.13, 7.65 and 7.51 ppm correspond respectively to H6, H4, H3 and H5 of the reduced, square planar *cis*-dichlorido Pt(II) complex (**3**), obtained upon losing the axial Cl$^-$ ligands. The chemical shift values of 9.08, 8.24 and 7.84 ppm correspond to H6, H4 and H3, respectively, of the hydrolyzed Pt(II) complex (**3a**, Scheme 3) as depicted in Fig. 2. The peak of H5 of the hydrolyzed product **3a** has similar chemical shift value (7.65 ppm) with the H3 of **3** as seen from the NMR plots (Fig. 2). The ESI-MS spectrum has also provided evidence for the formation of **3** and its hydrolyzed product along with the sodium or potassium ion bound to complex **1a** (Fig. S12†). The *m/z* value at 520.9330, 538.9435, 592.8755 and 608.8354 matches well with the species of formulation [**3** + Na$^+$]$^+$ (calcd 520.9429) (Table S3 and isotope modelling in Fig. S13†), [**3** + K$^+$]$^+$ (calcd 538.9160) (Table S3 and isotope modelling in Fig. S14†), [**1a** + Na$^+$]$^+$ (calcd 592.8788) (Table S3 and isotope modelling in Fig. S15†) and [**1a** + K$^+$]$^+$ (calcd 608.8527) (Table S3 and isotope modelling in Fig. S16†) respectively. The *m/z* corresponding to hydrolyzed complex **3** appeared at 462.9764 corresponding to the speciation [**3** − 2Cl$^-$ + 2OH$^-$ + H$^+$]$^+$ (calcd 463.0297) (Table S3 and isotope modelling in Fig. S17†). ESI-MS speciation indicates that both the Cl$^-$ might be lost upon hydrolysis. Further NMR studies presented later regarding the binding of 9-ethylguanine (9-EtG) confirm that upon monoaquation the reactivity towards nucleophilic substrates like 9-EtG may be initiated. One important point to note here is that the chemical shifts corresponding to the free aziridinium ion (of equatorial ligand L1, **3b**, Scheme 3) were found to be distinctly visible during our earlier work with **3** alone as the starting complex.[32] However in this case where **3** is generated *in situ* from **1a**, we
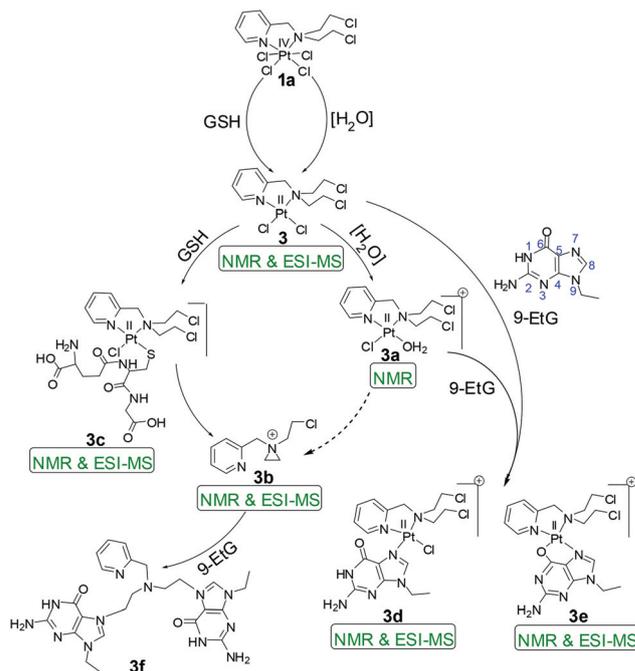
could see new peaks which may be due to aziridinium ion formation, but they did not appear distinctively and hence they cannot be assigned with certainty.

Complex **2a** showed hydrolysis right from the beginning and after 2 d most of the complex was hydrolyzed (Fig. S18†). Hence, it seems that the presence of the additional –CH$_2$CH$_2$Cl group on the bound nitrogen in **1a** has a positive effect on the kinetic stability of the Pt(IV) complex. This additional stability might be attributed to the change in the electronic factor especially the increase in steric hindrance. To understand the system further, it was now needed that a binding experiment with 9-EtG be performed. The objective was to find out if the binding of **1a** with guanine happens through the *in situ* formation of **3** and how many sites are hydrolyzed and accessible to 9-EtG per molecule of **1a**.

Interaction with model nucleobase and plasmid DNA

The binding studies of **1a** and **2a** with model nucleobase 9-EtG using the ^{1}H NMR technique provided better insight into the binding motif of the complexes with DNA. The binding studies were also performed in 20% PBS prepared in D$_2$O pD 7.4 in DMSO-d_6. N^7 of 9-EtG is the most likely position[58] of attack as evidenced from the chemical shift of the H8 proton of guanine (marked as H8$_G$) downfield. In our case we do not see the binding of complex **1a** directly with 9-EtG (added in a 1:6 molar ratio; 3 mM of **1a** & 18 mM of 9-EtG) although certain literature reports state that nucleobases can directly bind to Pt(IV).[22,59,60] The NMR data do not show any formation of free complex **3** or its aquated species rather we directly find
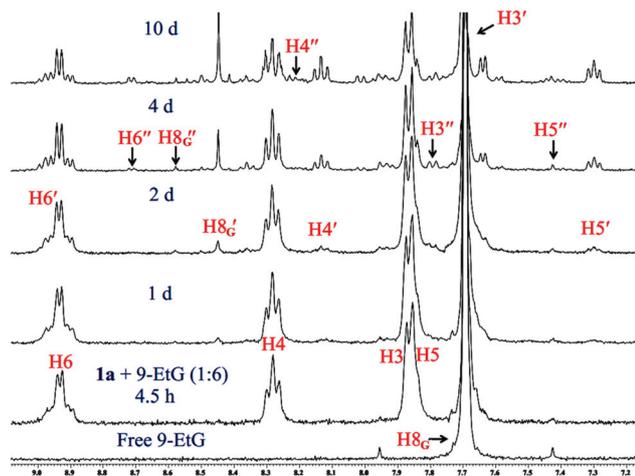
Fig. 3 Stack plot of ^{1}H NMR data obtained by the reaction of **1a** with 9-EtG (1 : 6) in 20% PBS (pD 7.4, prepared in D_2O) – DMSO-d_6 mixture. The chemical shifts depict the presence of excess reactants (**1a** & 9-EtG) and two types of 9-EtG bound adducts (**3d** & **3e**) after 10 d. H8$_G$ of free 9-EtG is shifted downfield to H8$'_G$ & H8$''_G$ of 9-EtG bound complexes **3d** & **3e** respectively.

the 9-EtG bound complex **3** after 2 d (Fig. 3). The above statement is made on the basis of the downfield shift of the H8$_G$ signal of 9-EtG from 7.69 ppm to 8.44 ppm (marked as H8$'_G$ in Fig. 3) due to the formation of a monoadduct of 9-EtG immediately upon the *in situ* formation of **3**.

The earlier depicted hydrolysis study with **1a** shows that the formation of the reduced Pt(II) complex **3** happens to have a very similar time scale as found for the 9-EtG bound speciation. Hence, the presence of 9-EtG during the formation of **3** might be immediately leading to the 9-EtG conjugation. The NMR data do not show any evidence of the formation of **3** or its aquated species in this case. However, this was not the case for our earlier studies with **3** as a starting compound,[32] where we could find evidence of both the 9-EtG adduct and hydrolyzed Pt(II) complex formation. This suggests that the kinetic pathway for DNA binding may not be the same *i.e.* the nucleophilic attack by 9-EtG may be taking place during the formation of the Pt(II) form leading to an activated intermediate which forms the 9-EtG bound Pt(II) adduct, without an intermediate hydrolysed Pt(II) species. It is also possible that the formation of the 9-EtG adduct is very quick after the aquation step hence the aquated species could not be observed. It should be borne in mind however, that the chemistry of the Pt(II) complex (**3**) presented earlier[32] does not support such a fast 9-EtG binding upon aquation hence the above prediction about the difference in the reaction pathway is made.

The binding of 9-EtG is well supported by the ESI-MS results from the same experiment, under ESI-MS conditions we also find the Pt(II) diaquated species as per the *m/z* peak of 462.9832 (calcd 463.0297) corresponding to $[3 - 2Cl^- + 2OH^- + H^+]^+$ (Fig. S19, Table S3†). Since the intensity is low for the diaquated species and we do not find it in NMR hence we feel that the small amount of diaquated species is a result of spe-

ciation arising under the ESI-MS conditions. We could find the most intense *m/z* at 642.0576 which matches well with the mono-guanine adduct of formulation $[(1a - 3Cl^-) + 9\text{-EtG}]^+$ (calcd 642.0657) (Fig. S19, Table S3 and isotope modelling at Fig. S20†). The H8$'_G$ singlet is in good resemblance with the singlet found in the binding experiment of **3** with 9-EtG (1 : 3 molar ratio) maintaining the same experimental conditions.[32] The singlet at 8.57 ppm (marked as H8$''_G$ in Fig. 3) corresponding to the scarcely found N^7, O^6 chelation of 9-EtG with **3** (**3e**, Scheme 3) was also observed but in a low amount.[32,61,62] However, it must be noted that such a chelated adduct may be difficult to form under *in vivo* conditions when the guanine is part of a DNA strand. The small amount of the chelated adduct formation is also found in ESI-MS at a *m/z* of 606.0793 (calcd 606.0896) corresponding to formulation $[(3 - 2Cl^-) + (9\text{-EtG} - H^+)]^+$ (Table S3 and isotope modelling in Fig. S21†). The peaks corresponding to the pyridyl protons (H6, H4 H3, H5) for both the 9-EtG adducts, **3d** and **3e** appeared at (8.96, 8.15, 7.71, 7.31) and (8.73, 8.23, 7.78, 7.41) ppm respectively. The aliphatic region of the binding kinetics also contains the signals corresponding to **3d** & **3e**, but there is a merging of signals leading to poor resolution although we could identify most of them (Fig. S22†).

The 2D NMR (HMQC) of the reaction mixture was performed at two different time points (10 min and 10 d) in order to obtain more clarity on the speciation and comment on the certainty of the signals from the bound species **3d** & **3e** respectively. The plots of NMR data are summarized in Fig. S23–S37 and Table S4A, S4B.† The experimental results support the predicted adducts **3d** & **3e** along with some other species that cannot be assigned properly. Since we used higher concentrations of **1a** (15 mM) and 9-EtG (90 mM) it was possible to obtain information which we missed earlier. Herein we could find a signal of H8$'_G$ just after the mixing of 9-EtG with **1a** suggesting that a small amount of the adduct is formed right after mixing (Fig. S23†). The fact that the speciation is in a very small amount is more evident since we could not obtain any ^{13}C signal (Fig. S24†) or a correlation spectrum (Fig. S25 and S26†) for the same. We observed a downfield shift of the protons (Fig. S27 and S28†) and carbons (Fig. S29–S33†) of unreacted 9-EtG after 10 d which is not completely understood but may be due to the insufficiency of the buffer capacity of the reaction mixture.

The ^{195}Pt NMR studies of the 9-EtG binding with **1a** also provide support for the generation of predicted adducts **3d** & **3e**. Since the 9-EtG adduct formation is slow to generate the minimum signal to noise ratio, which is needed for the adducts to be visible, we probed the adduct formation after 10 days and found a tiny signal for the ^{195}Pt chemical shift at *ca.* −2210 ppm which does not provide enough resolution to distinguish between **3d** & **3e**. The major species remains to be the parent complex **1a** (^{195}Pt at −74.7 ppm, Fig. S38†) displaying a higher stability for **1a** as compared to **3**.

To our surprise complex **2a** showed faster hydrolysis but no trace of 9-EtG binding up to 2 days in 20% PBS (Fig. S39†). After 2 days most of the complex was found to be hydrolyzed, yet no new peak for H8 of 9-EtG corresponding to the binding

was observed and hence, no more data were recorded. However, in the presence of plasmid DNA (pUC19) **2a** showed more interaction than **1a** (Fig. S40A†), suggesting that the affinity for 9-EtG may not be strong enough but it may interact with a plasmid DNA having multiple targets. It would appear that **2a** should be more toxic however, the faster reactivity of **2a** may prohibit its cellular uptake due to binding with other potential nucleophiles in the assay solution. Cisplatin showed more retardation of DNA at similar concentrations (Fig. S40A†). We could see that there is some amount of cleavage of DNA as per the gel diagram which may be during the reduction of the Pt(IV) to Pt(II) species in the solution. The amount of the cleavage product observed is in the order **1a** > **2a**. For cisplatin the cleavage product is similar to the control. The cleavage of DNA seems ROS based since when GSH is used there is no more cleavage to be found (Fig. S40B†). In addition the retardation has also decreased suggesting the interference of GSH with the DNA binding.[63] However, the cytotoxicity assay performed in the presence of at least 30 equivalents of GSH showed that the decrease in cytotoxicity is not much (details in cell viability studies).

Interaction with glutathione and ascorbate

Glutathione (GSH), the cellular thiol containing tripeptide, is responsible for the drug resistance of platinum drugs[64,65] and also contributes in the bio-reduction of various prodrugs including Pt[66–68] and Ru[69,70] drugs. Pt(IV) drugs are reduced to Pt(II) by GSH after the removal of their axially coordinated ligands. Our results also show that complex **1a** loses its axial chloro group and gets transformed into the Pt(II) analogue (**3**) almost instantaneously upon mixing with GSH (1 : 6 molar ratio, monitored by ^{1}H NMR) in 20% PBS (pD 7.4, prepared in D_2O) in DMSO-d_6 (Fig. 4). Careful observation suggests that the transformation could be visualized by the naked eye through fading of the yellow colour of the Pt(IV) solution rendering a faint yellow solution corresponding to the Pt(II) species (**3**). Each GSH molecule would contribute one electron
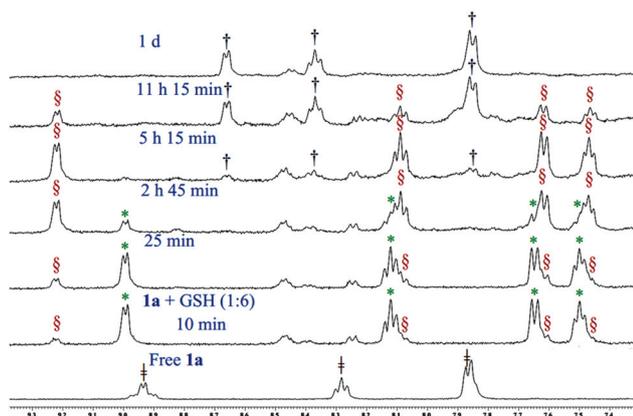
Fig. 4 Stack plot of ^{1}H NMR data obtained by the reaction of **1a** with GSH (1 : 6) in 20% PBS (pD 7.4, prepared in D_2O) – DMSO-d_6 mixture, where ‡, *, § and † indicate the signals of intact complex **1a**, **3**, GSH bound complex **3c** and aziridinium ion **3b** respectively.

to the reduction process. The final product of the reduction would be a Pt(II) species (**3**), two molecules of HCl and one molecule of oxidized glutathione (GSSG). After the reduction, the *in situ* generated Pt(II) complex (**3**) starts to form a GSH adduct at a faster pace. It is also evident from the binding experiments that the complex only forms a monoadduct of GSH (**3c**, Scheme 3). The chemical shifts for the GSH bound adduct are 9.22, 8.10, 7.62 and 7.46 ppm for H6, H4, H3 and H5 type protons, respectively (Fig. 4). Mass spectral evidence provides additional support to the NMR data suggesting the formation of a mono-adduct of GSH with the Pt(II) species (Fig. S41†). The corresponding m/z value of 770.0723 matches well with the species $[(3 - Cl^-) + (GSH - H^+) + H^+]^+$ (calcd m/z 770.0688) (Table S3 and isotope modelling at Fig. S42†). The sodium ion containing m/z corresponds to the proposed adduct where 792.0598 shows a good match with the formulations $[(3 - Cl^-) + (GSH - 2H^+ + Na^+) + H^+]^+$ (calcd 792.0508) (Table S3 and isotope modelling at Fig. S43†). However, the ESI-MS data provide an additional peak at a m/z of 734.0967 (calcd 734.0927) which corresponds to the S, N– chelated GSH bound Pt(II) after the replacement of both the chlorido ligand of Pt(II) species, $[(3 - 2Cl^-) + (GSH - H^+)]^+$ as shown in Table S3 and isotope modelling in Fig. S44.† This species is not observed in NMR and although ESI-MS conditions are softer, yet the formation of this chelated GSH species may be under ESI-MS conditions. The oxidation of GSH is also supported by the ESI-MS through the observation of a m/z of 613.1584 (calcd 613.1598) and 635.1370 (calcd 635.1417) signifying the formulation to be $[GSSG + H^+]^+$ and $[GSSG + Na^+]^+$ respectively (Table S3 and isotope modelling at Fig. S45, S46†). The GSH binding was completed at around 5 h, then the peaks corresponding to the adduct started to diminish and new peaks corresponding to the aziridinium ion of L1 emerged in the NMR plot at 8.67, 8.37 and 7.86 ppm (Fig. 4, for H6, H4 and H3 (merged with H5) protons respectively). After a day all the GSH adduct peaks disappeared as observed in our earlier work.[32] Since the GSH bound species formed *in situ* is the same hence we attribute it to the same cause as earlier. The release of the L1 ligand is due to the high *trans* effect of the S-donor of coordinated GSH in the GSH adduct which labilizes the coordinated nitrogen mustard moiety L1 resulting in an aziridinium ion. Hence, complex **1a** reduced to Pt(II) complex **3**, then was bound to GSH and finally dissociated to form the free aziridinium ion (**3b**, Scheme 3). The aliphatic region of the GSH binding is too complicated as most of the peaks corresponding to **3**, **3b** or **3c** are merged within the peaks of GSH or oxidized GSH (Fig. S47†) and hence not mentioned in the discussion. In addition the released Pt(II) might form a S bridged polymeric Pt species[71] which corroborates with our earlier evidence.[32] Hence, only the peaks corresponding to this aziridinium ion were visible. We did not see any peaks corresponding to the Pt species as commented on in the literature and we also do not observe any precipitate in the solution used.[71] The ESI-MS data (Fig. S48†) also support the formation of the aziridinium ion exhibiting a m/z of 197.0805 (calcd 197.0845) (Table S3 and isotope modelling at Fig. S49†). In

Paper

addition we observe the GSH m/z to be 308.0923 (calcd 308.0916) (isotope modelling at Fig. S50†) and its oxidized species with a m/z of 613.1584 and 635.1491 corresponding to $[\text{GSSG} + \text{H}^+]^+$ (calcd 613.1598) (isotope modelling at Fig. S51†) and $[\text{GSSG} + \text{Na}^+]^+$ (calcd 635.1417) (isotope modelling at Fig. S52†) respectively. Hence, the ESI-MS data corroborate well with the NMR observations signifying that the Pt(II) from the decomposed **3** might have formed a S bridged polymeric Pt species.

[195]Pt NMR spectra were also in accordance with the reduction of **1a** by GSH to form **3** followed by the formation of **3c** and vanishing of the NMR signal (Fig. S53†) due to the formation of polymeric species.

We have also checked the reduction reaction of complex **1a** with ascorbic acid (1 : 6 molar ratio) by proton NMR under the same conditions as followed for GSH. We found that here too the reduction of **1a** to **3** was very fast as found for GSH. We only obtained the peaks corresponding to the Pt(II) complex (**3**) within 10 minutes of mixing with ascorbic acid which degrades to the aziridinium ion within 10 h (Fig. S54 and S55†).

Cell viability studies

Complexes **1a** & **2a** were probed for *in vitro* cytotoxicity against various cancerous cell lines. The studies of **1a** against MCF-7, A549, HepG2 & MIA PaCa-2, non-tumor (HEK293) and non-tumorigenic mouse fibroblast (NIH 3T3) cell lines under normoxic conditions showed **1a** to be most toxic to MIA PaCa-2 (IC_{50} = 4.4 ± 0.5 μM, $p < 0.05$), although it is also potent with IC_{50} in the range of *ca.* 8–18 μM for MCF-7, A549, HepG2, HEK293 and NIH 3T3. The dose response of **1a** in MIA PaCa-2 was seven fold better than cisplatin (IC_{50} = 31.8 ± 4.8 μM, $p < 0.05$) under our experimental conditions (Table 1).

The *in vitro* cytotoxicity studies of **2a** against MCF-7 and A549 showed that it is not toxic up to 100 μM. The kinetic instability may be one of the reasons for the poor cytotoxic profile of **2a**, it may be decomposing fast as it encounters the culture media components and hence fails to reach the cellular target. In addition as per the NMR studies, upon hydrolysis **2a** does not show any binding to the model nucleobase 9-EtG. Hence no more cytotoxicity experiments were carried out with **2a**.

All the IC_{50} values determined for **1a** were compared with the IC_{50} value of **3** (Table 1) in an urge to know the dependence of cytotoxicity (IC_{50} values) on the alteration of the oxidation state from **3** to **1a**. Among the tested cell lines the highest toxicity exhibited by **1a** was against MIA PaCa-2 (IC_{50} = 4.4 ± 0.5 μM, $p < 0.05$) which is comparable with the IC_{50} (4.2 ± 1.0 μM, $p < 0.05$) of **3**. In HepG2 also both **1a** and **3** showed similar IC_{50} of 8.6 ± 0.6 μM ($p < 0.05$) and 8.8 ± 0.3 μM ($p < 0.05$) respectively. Similarly in the case of MCF-7 and A549 no alterations of IC_{50} were found between **1a** and **3**. Hence it can be stated that derivatization from the kinetically labile Pt(II) to apparently kinetically inert Pt(IV) showed almost no effect in terms of the cytotoxicity profile but there was improvement in the solution stability profile under similar conditions.

The cytotoxicity pattern of **1a** in HEK293 is even better than **3**. It is known that HEK293 overexpresses two human copper

Table 1 Cytotoxicity data of **1a**, **2a**, **3** and cisplatin

	Normoxia[b]								Hypoxia[c]					
$IC_{50} \pm SD^a$ (μM)	MCF-7	MCF-7 + GSH	A549	A549 + GSH	HepG2	MIA PaCa-2	HEK293	NIH 3T3	MCF-7	MCF-7 + GSH	A549	A549 + GSH	MIA PaCa-2	MIA PaCa-2 + GSH
1a	11.4 ± 2.0	12.9 ± 1.2[d]	18.2 ± 1.0	24.1 ± 1.5[d]	8.6 ± 0.6	4.4 ± 0.5	8.6 ± 2.3	8.8 ± 1.2	8.6 ± 0.8	11.2 ± 1.8[d]	16.1 ± 1.1	26.3 ± 2.5[d]	3.3 ± 0.2	4.5 ± 0.3[d]
2a	>100	>100	>100	>100	ND[e]	ND[e]	ND[e]	ND[e]	>100	>100	>100	>100	ND[e]	ND[e]
3	12.6 ± 0.8[f]	16.4 ± 1.2[f]	18.2 ± 1.8[f]	31.2 ± 4.2[f]	8.8 ± 0.3	4.2 ± 1.0[f]	14.9 ± 0.8[f]	6.8 ± 0.5	9.4 ± 2.2[f]	12.5 ± 1.1[f]	20.8 ± 1.5[f]	26.6 ± 3.5[f]	3.4 ± 0.2[f]	4.4 ± 0.4[f]
Cisplatin	14.1 ± 1.2[f]	27.8 ± 2.1[f]	22.8 ± 1.2[f]	41.3 ± 1.5[f]	14.3 ± 0.8	31.8 ± 4.8[f]	>50[f]	7.0 ± 1.0	18.7 ± 1.4[f]	29.0 ± 1.1[f]	24.4 ± 1.1[f]	39.3 ± 1.3[f]	18.1 ± 2.9[f]	29.7 ± 4.1[f]

[a] SD means standard deviation, IC_{50} values were calculated by nonlinear curve fitting in dose response inhibition – variable slope model using Graph pad prism, the data presented have significance (p value) less than 0.05 or better; Cell lines: MCF-7 (human breast adenocarcinoma), A549 (human lung carcinoma), HepG2 (human hepatocellular carcinoma), MIA PaCa-2 (human pancreatic carcinoma), HEK293 (human embryonic kidney), NIH 3T3 (mouse embryonic fibroblast). [b] IC_{50} was determined under normoxic conditions. [c] IC_{50} was determined under hypoxic conditions (1.5% O_2). [d] The amount of GSH used in all cases was 400 μM. [e] ND means not determined. [f] Data are taken from ref. 32.

transporting ATPases (ATP7A & ATP7B),[72] which are responsible for the efflux of cisplatin.[73–77] The ligand environment around **1a** or its reduced form (**3**) might have prohibited the ligation through the cys rich region of ATP7A & ATP7B due to the enhanced steric factor rendering better activity against that particular cell line. Earlier also we have observed a higher cytotoxicity of the Pt(II) analogue (**3**, IC_{50} = 14.9 ± 0.8 μM, $p < 0.01$) but the activity of **1a** is better (IC_{50} = 8.6 ± 2.3 μM, $p < 0.05$). This might be because the higher solution stability of **1a** is due to its relatively kinetically inert nature which made the de-activation further difficult.

The cytotoxicity profile of **1a** when compared in non-tumorigenic mouse fibroblast (NIH 3T3) *vs.* MIA PaCa-2 showed that the IC_{50} in NIH 3T3 needs double the dosage than that against MIA PaCa-2. This is encouraging, although it should be still better, for a good anticancer agent. In addition it must be noted that the *in vitro* cytotoxicity of the clinical drug cisplatin in NIH 3T3 is also similar to that of **1a** (Table 1) although **1a** is more efficient in MIA PaCa-2.

Although the above data are encouraging the indifference of the effect of the kinetic inertness found in the *in vitro* activity led us to probe the effect of the cytotoxicity of **1a** in the presence of GSH. NMR studies showed that **1a** gets almost instantly converted to its Pt(II) analogue (**3**) in the presence of GSH and also binds with GSH. Hence it seemed that detoxification of **1a** by GSH is inevitable. To evaluate this we have determined the IC_{50} of **1a** in the presence of an excess amount of GSH (400 μM) against MCF-7 and A549 under normoxic conditions. In both the cell lines (MCF-7 and A549) the IC_{50} of **1a** showed an increase in the dosage amount but the activity was still better than that observed for **3** or cisplatin (Table 1). The above results suggest that **1a** may be converted to **3** but the reactivity towards GSH may not follow the same trend as found in the NMR experiment.

We have also studied the cytotoxicity of **1a** under hypoxic conditions against MCF-7, A549 and MIA PaCa-2 in the presence and absence of excess GSH. The IC_{50} value in the absence of excess added GSH showed that the cytotoxic activity of **1a** stays similar or is better than normoxic conditions (Table 1) signifying that the activity of **1a** inside a tumor may not be hindered due to hypoxia. On addition of excess GSH (400 μM) compared to the respective complexes we find that the activity of **1a** worsens but the dosage is still similar to the normoxic IC_{50} values without any added GSH especially for the MIA PaCa-2 and MCF-7 cell lines (Table 1). The activity is comparatively poorer for the A549 cell line which shows that the compound is not active against all cancer cell lines. Cisplatin shows much worsening of the activity against A549, compared to **1a** (Table 1) under similar conditions. In MIA PaCa-2 although the activity of cisplatin in hypoxia is better yet a *ca.* 6 times higher dosage than **1a** is required.

Cellular internalization and mechanistic studies

The accumulation study of the metal in the cancer cells is known to provide insight about the internalization of a given complex.[78] We used the ICP-MS technique to quantify the amount of Pt in the cancer cells after 24 h of exposure with equal concentrations (9 μM) of each complex. **1a** shows a higher uptake based on the Pt content inside MCF-7 cells, compared to **2a** (Fig. 5). The platinum accumulation of **2a** is significantly less than even cisplatin or the reduced Pt(II) complex **3**. This is in good agreement with the lower IC_{50} values of **1a**. The slow hydrolysis of **1a** helps to keep it neutral and hence renders a greater lipophilic character which might be acting in favour of greater internalization.

Complex **1a** was probed to gain insight about its effect on the cell cycle. Flow cytometry data show that **1a** arrests the MCF-7 cell cycle most prominently in the G2/M phase after 24 h exposure of **1a**, which is observed by an increase of the population in this phase with an increasing concentration of **1a** w.r.t. untreated control cells (Fig. 6 & S60†). The G2/M phase arrest was also found for MIA PaCa-2 but the effect was less pronounced in MIA PaCa-2 compared to MCF-7 (Fig. 6 & S61†).

The efficiency of **1a** led us to probe if the killing pathway is apoptotic in nature. DNA extracted from MCF-7 cells treated
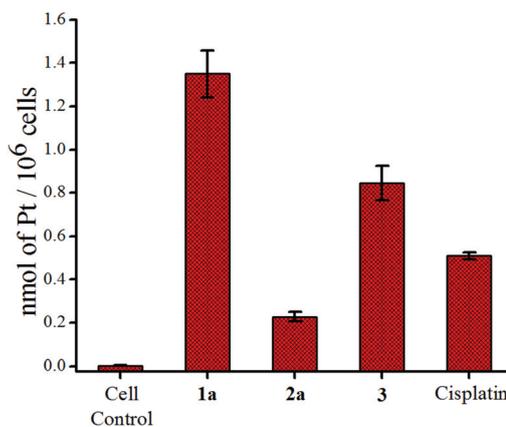
Fig. 5 Accumulation of platinum in MCF-7 cells after treatment with 9 μM of **1a**, **2a**, **3** and cisplatin respectively.
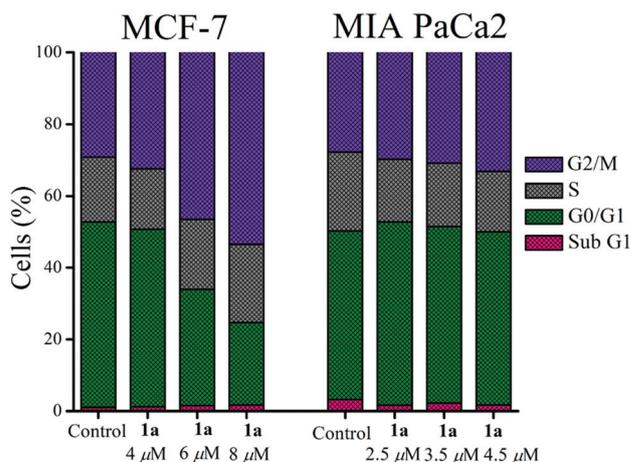
Fig. 6 Cell cycle arrest by **1a** showing G2/M phase arrest both in MCF-7 and MIA PaCa-2.

with sub IC$_{50}$ concentrations of **1a** (6 μM, 8 μM and 10 μM respectively) for 24 h showed a ladder pattern in agarose gel electrophoresis, while intact DNA was observed for the untreated cells (Fig. 7). The above results suggest that **1a** kills through apoptosis since inter-nucleosomal DNA fragmentation[79,80] with sections of around 180 bp of endonucleases is a hallmark of apoptosis.[81–83]

The apoptotic pathway was further strengthened by probing the change in mitochondrial transmembrane potential and caspase activation as described below. Among the two major pathways of apoptosis, the intrinsic mechanism is regulated *via* mitochondria.[84,85] In this event the mitochondrial membrane potential (ΔΨ_m) disintegrates.[86] We could observe a significant change in the mitochondrial membrane potential by **1a**, using the mitochondria specific fluorescent dye JC-1. The JC-1 dye emits red fluorescence (λ_{ex} = 575 nm, λ_{em} = 590 nm) when the mitochondrial membrane is intact with the usual ΔΨ_m (since JC-1 remains in aggregates) and when the membrane potential is no longer intact it emits green fluorescence (λ_{ex} = 510 nm, λ_{em} = 550 nm) due to the monomeric form.[87] Therefore, a decrease in the ratio of the red/green fluorescence intensity of JC-1 reflects depolarization of the mitochondrial membrane potential.[88] The strong depolarization of the mitochondrial membrane potential by **1a** shows concentration dependence (Fig. 8) with respect to untreated MCF-7 cells determined by flow cytometry. This may be taken as an indication that **1a** possibly goes through an intrinsic pathway which involves depolarization of the mitochondrial membrane potential.

The release of cytochrome c into the cytoplasm is triggered by the depolarization of the mitochondrial membrane poten-
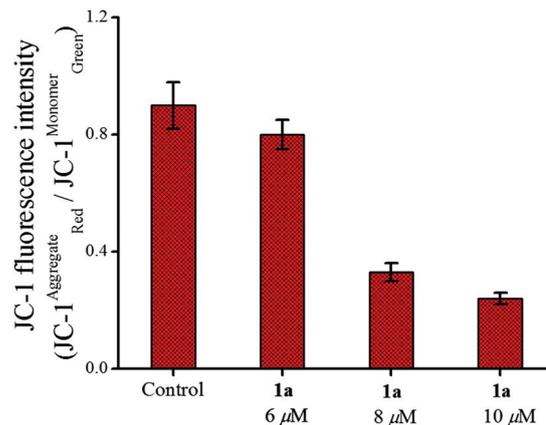
Fig. 8 Change in the mitochondrial membrane potential of MCF-7 cells after treatment with **1a** over 24 h showing the effect of increasing concentration.

tial which in turn activates initiator (*e.g.* caspase-9) and effector (*e.g.* caspase-7) caspases leading to cell death after proteolytic cleavage of a wide range of cellular targets.[89,90] Our initial studies in this area show that caspase-7 (cleaves Ac-DEVD-pNA substrate)[91] was activated in MCF-7 by 24 h of treatment with **1a** (Fig. 9) and this activation also showed concentration dependence as found from the plot of the pNA released (nmol min^{-1} ml^{-1}) *vs.* the concentration used.

One more characteristic of apoptosis is causing cellular morphological changes that include cell shrinkage, plasma membrane blebbing and chromatin condensation.[92] The above signatures of apoptosis were also observed for the **1a** treated MCF-7 cells (Fig. S62†) using DAPI staining while the cells from the control experiment remained intact.

The above studies including DNA ladder formation, depolarization of the mitochondrial membrane potential, caspase activation and nuclear morphological changes strongly suggest that the cells are killed through an apoptotic pathway by **1a**.
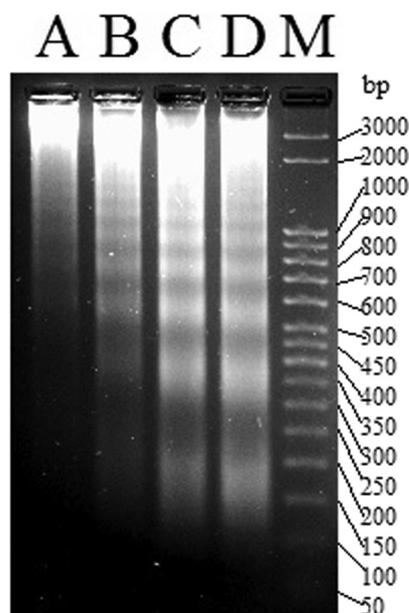
Fig. 7 Gel image of the DNA ladder formation of MCF-7 treated with (A) DMSO, (B) 6 μM of **1a**, (C) 8 μM of **1a** and (D) 10 μM of **1a** respectively over 24 h. M denotes the known bp ladder.
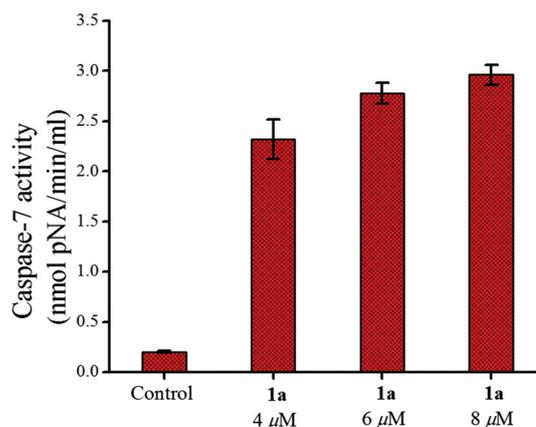
Fig. 9 Caspase-7 activity in MCF-7 cells after treatment with **1a** over 24 h showing the enhancement of activity with an increase in concentration.

Growth kinetics of MCF-7 under the influence of 1a

We had a quest as chemists that what is the fate of the cells after removal of the anticancer agents. We were curious and relevant data appeared to be scarce.[93] We incubated the MCF-7 cells with **1a** for 48 h. The results showed that the cells ceased to grow, even after removal of **1a** and the effect was observed until 48 h (Fig. 10). The clinical drug cisplatin also showed similar behaviour as **1a** in this experiment. Hence, the decrease in viability is encouraging and indicative that compound **1a** imposes a permanent damage in the cancer cells ceasing its growth even after the drug-removal.

Wound assay (migration)

Migration is an essential property exhibited by cells in order to safeguard tissue functions, wound healing and related processes. It also plays a predominant role in several diseases, especially in cancer, leading to invasion and metastasis.[94]
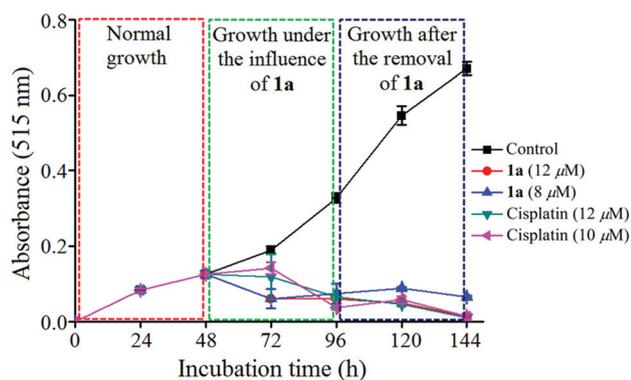
Fig. 10 Plot of growth kinetics of MCF-7 under the influence of **1a** determined by MTT assay.
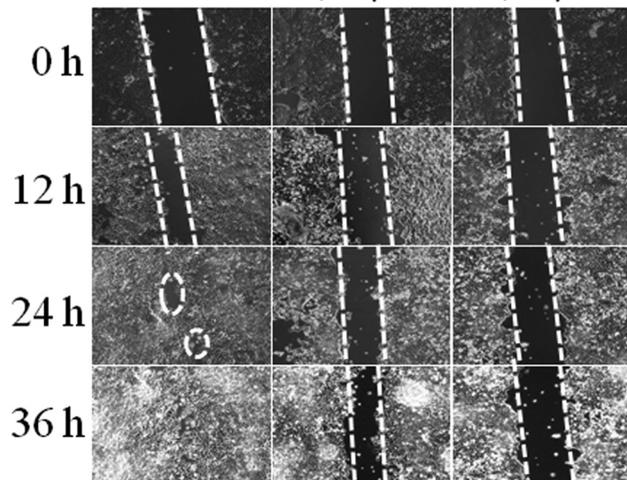
Fig. 11 Wound healing assay in MCF-7 cells where untreated cells move rapidly towards the scratched area with an increase in time as compared to cells treated with 6 & 8 µM of **1a** respectively.

Therefore the effect of **1a** on cancer cell migration in the MCF-7 cell line was assessed using the scratch wound healing assay. From Fig. 11 it can be seen that the untreated control cells rapidly migrate over time due to the metastatic property resulting in almost full healing in 36 h. Whereas in the case of **1a** added cells the wide denuded area remained mostly unhealed, indicating the anti-proliferative nature of the cells, attained upon treatment with **1a**.

In addition to the above **1a** was found to have a very much tolerant level for hemolysis[95–97] as found from its interaction with blood components particularly RBCs (using 15 µM of **1a**, hemolysis was <2.1%, Fig. S63 & Table S5†). Hence, complex **1a** appears to be a blood compatible, cytotoxic and anti-metastatic anticancer agent.

Conclusions

In a single step the Pt(II) to Pt(IV) conversion was achieved along with the generation of nitrogen mustards from the co-ordinated ethanolamine/diethanolamine moiety. The direct coordination of the nitrogen mustard to kinetically inert Pt(IV), is scarce, and very much increases the solution stability compared to the Pt(II) analogue. The bis(2-chloroethyl)amine moiety in **1a** ensures the provision of the required electronic factors which allow binding to 9-EtG, higher cytotoxicity and solution stability compared to **2a**, which has the 2-chloroethylamine moiety. The dose effectiveness of **1a** was detected even in the presence of excess GSH, unlike cisplatin. A prominent G2/M phase arrest by complex **1a** is noticed in two different cell lines, MCF-7 and MIA PaCa-2. The *in vitro* data against MCF-7 also suggest that **1a** induces the loss of the mitochondrial membrane potential and caspase-7 activation leading to apoptosis. In addition an initial study on the anti-metastatic properties of **1a** shows a positive effect, which confirms it to be a potential candidate as an anticancer agent. We have gained a better understanding of the chelating nitrogen mustard bearing Pt(II/IV) complexes, revealing appreciable *in vitro* cytotoxicity profiles, which are getting fine tuned with our progress.

Experimental section

Materials and methods

The solvents and chemicals used were purchased from various authentic commercial sources. 9-EtG and GSH were purchased from Carbosynth and used as received. Analytical grade solvents were purchased from Merck India and distilled prior to use. Spectroscopy grade solvents (Spectrochem) were used in spectroscopic studies. 3-(4,5-Dimethyl-2-thiazolyl)-2,5-diphenyl-2*H*-tetrazolium bromide (MTT), 4′,6-diamidino-2-phenylindole dihydrochloride (DAPI) and penicillin–streptomycin were purchased from USB and Hyclone respectively. Dulbecco's Modified Eagle's Medium (DMEM), Minimum Essential Medium (MEM) and Phosphate-Buffered Saline (PBS) were

Paper

purchased from Invitrogen. 5,5′,6,6′-Tetrachloro-1,1′,3,3′-tetra-ethylbenzimidazolylcarbocyanine iodide (JC-1) and propidium iodide (PI) were purchased from Sigma-Aldrich. UV–visible data were recorded using a Perkin Elmer lambda 35 spectrophotometer. FT-IR spectra were recorded using a Perkin-Elmer SPECTRUM RX I spectrometer in KBr pellets. ^{1}H & ^{13}C (proton decoupled) and ^{195}Pt (proton coupled) NMR spectra of the complexes were recorded using a Bruker Avance III 500 MHz spectrometer at room temperature. All chemical shifts are reported in parts per million (ppm). ^{195}Pt NMR chemical shifts are described against the standard $K_2[PtCl_4]$ for which the chemical shift in D_2O is at −1628.0 ppm. Elemental analyses reported were performed using a Perkin-Elmer 2400 series II CHNS/O analyzer. Electrospray ionization mass spectra (ESI-MS) were performed using a Micromass Q-Tof micro™ (Waters) by +ve mode electrospray ionization. The synthetic yields reported are of isolated analytically pure compounds.

cis,cis,trans-[Pt(L1)Cl$_4$] (1a). 1[32] (0.45 g, 0.97 mmol) was added to 5 mL of $SOCl_2$, the solution turned quickly to deep yellow along with a solid suspension. The reaction mixture was allowed to stir for an additional 8 h. After filtration the yellow solid was washed thrice with dry toluene followed by DCM and finally dried under vacuum. Yield 0.55 g (96%). Single crystals suitable for X-ray diffraction were obtained after layering of the HCl acidified acetonitrile solution with pet ether for 3 days. ^{1}H NMR (500 MHz, DMSO-d_6) δ: 8.99 (d, 1H, J = 5.5 Hz, ^{195}Pt satellites, $^3J_{H-Pt}$ = 26.3 Hz, PyH6), 8.38 (td, 1H, J_1 = 7.6 Hz, J_2 = 1.2 Hz, PyH4), 7.94–7.89 (m, 2H, PyH3 & PyH5), 5.10 (s, 2H, ^{195}Pt satellites, $^3J_{H-Pt}$ = 17.5 Hz, PyCH$_2$N), 4.17 (t, 4H, J = 7 Hz, CH$_2$Cl), 3.82–3.70 (m, 4H, CH$_2$N); ^{13}C NMR (125 MHz, DMSO-d_6) δ: 159.2 (PyC2), 147.6 (PyC6), 143.6 (PyC4), 127.3 (PyC5), 124.9 (PyC3), 68.8 (PyCH$_2$N), 59.6 (CH$_2$N), 38.0 (CH$_2$Cl); ^{195}Pt NMR (107.5 MHz) δ: −64.1; elemental analysis calcd (%) for $C_{10}H_{14}Cl_6N_2Pt$: C 21.07, H 2.48, N 4.91, found: C 21.01, H 2.44, N 4.86; FT-IR (KBr, cm^{-1}): 2922 (w), 1612 (w), 1500 (w), 1463 (m), 1425 (m), 1304 (w), 1257 (w), 1061 (w), 968 (w), 768 (s); UV–vis in MeCN [λ_{max}, nm (ε, M^{-1} cm^{-1})]: 238 (14040), 268 (9800), 302 (3710).

cis,cis,trans-[Pt(L2)Cl$_4$] (2a). 2 was prepared from (2-hydroxy-ethyl)pyridylmethylamine[98] following the same method as 1. 2 was converted to 2a utilizing the similar procedure as 1a. Yield (92%). ^{1}H NMR (500 MHz, DMSO-d_6) δ: 9.09 (d, 1H, J = 6.5 Hz, ^{195}Pt satellites, $^3J_{H-Pt}$ = 26.3 Hz, PyH6), 8.76 (br, 1H, NH), 8.32 (td, 1H, J_1 = 7.75 Hz, J_2 = 1.3 Hz, PyH4), 7.94 (d, 1H, J = 7.5 Hz, PyH3), 7.88 (t, 1H, J = 6 Hz, PyH5), 4.93 (m, 1H, PyCH$_2$N), 4.67 (m, 1H, $^3J_{H-Pt}$ = 18.7 Hz, PyCH$_2$N), 4.09 (t, 2H, J = 7 Hz, CH$_2$Cl), 3.8–3.77 (m, 2H, CH$_2$N); ^{13}C NMR (125 MHz, DMSO-d_6) δ: 160.8 (PyC2), 146.9 (PyC6), 142.9 (PyC4), 126.8 (PyC5), 123.7 (PyC3), 60.5 (PyCH$_2$N), 54.7 (CH$_2$N), 38.7 (CH$_2$Cl); ^{195}Pt NMR (107.5 MHz) δ: −174.0; elemental analysis calcd (%) for $C_8H_{11}Cl_5N_2Pt$: C 18.93, H 2.18, N 5.52, found: C 18.86, H 2.21, N 5.58; FT-IR (KBr, cm^{-1}): 3441 (br), 2369 (w), 1629 (w), 1425 (w), 1230 (s), 1060 (m), 1017 (s), 770 (m), 584 (w); UV–vis in MeCN [λ_{max}, nm (ε, M^{-1} cm^{-1})]: 237 (11160), 418 (470).

The full details of the experimental procedures followed are given in the ESI.†

Statistical analysis

All data were given as the mean of independent experiments. The statistical analyses were analyzed using Graph pad prism® software 5.0 with Student's *t*-test.

Acknowledgements

Notes and references

1 B. Rosenberg, L. Van Camp and T. Krigas, *Nature*, 1965, **205**, 698–699.
2 B. Rosenberg, L. VanCamp, J. E. Trosko and V. H. Mansour, *Nature*, 1969, **222**, 385–386.
3 B. Rosenberg and L. VanCamp, *Cancer Res.*, 1970, **30**, 1799–1802.
4 C. A. Rabik and M. E. Dolan, *Cancer Treat. Rev.*, 2007, **33**, 9–23.
5 P. J. O'Dwyer, J. P. Stevenson and S. W. Johnson, *Cisplatin*, 1999, 31–69.
6 M. A. Jakupec, M. Galanski and B. K. Keppler, *Rev. Physiol., Biochem. Pharmacol.*, 2003, **146**, 1–53.
7 L. Kelland, *Nat. Rev. Cancer*, 2007, **7**, 573–584.
8 N. Pabla and Z. Dong, *Kidney Int.*, 2008, **73**, 994–1007.
9 P. J. O'Dwyer, J. P. Stevenson and S. W. Johnson, *Drugs*, 2000, **59**, 19–27.
10 S. R. McWhinney, R. M. Goldberg and H. L. McLeod, *Mol. Cancer Ther.*, 2009, **8**, 10–16.
11 J. H. Van Den Berg, J. H. Beijnen, A. J. M. Balm and J. H. M. Schellens, *Cancer Treat. Rev.*, 2006, **32**, 390–397.
12 L. R. Kelland, *Drugs*, 2000, **59**, 1–8.
13 P. Heffeter, U. Jungwirth, M. Jakupec, C. Hartinger, M. Galanski, L. Elbling, M. Micksche, B. Keppler and W. Berger, *Drug Resist. Updates*, 2008, **11**, 1–16.
14 B. Koeberle, M. T. Tomicic, S. Usanova and B. Kaina, *Biochim. Biophys. Acta, Rev. Cancer*, 2010, **1806**, 172–182.
15 N. J. Wheate, S. Walker, G. E. Craig and R. Oun, *Dalton Trans.*, 2010, **39**, 8113–8127.
16 B. W. Harper, A. M. Krause-Heuer, M. P. Grant, M. Manohar, K. B. Garbutcheon-Singh and J. R. Aldrich-Wright, *Chem. – Eur. J.*, 2010, **16**, 7064–7077.
17 A. Eastman, *Cancer Cells*, 1990, **2**, 275–280.
18 Z. H. Siddik, *Oncogene*, 2003, **22**, 7265–7279.

19 M. D. Hall and T. W. Hambley, *Coord. Chem. Rev.*, 2002, **232**, 49–67.

20 N. Graf and S. J. Lippard, *Adv. Drug Delivery Rev.*, 2012, **64**, 993–1004.

21 E. E. Blatter, J. F. Vollano, B. S. Krishnan and J. C. Dabrowiak, *Biochemistry*, 1984, **23**, 4817–4820.

22 O. Novakova, O. Vrana, V. I. Kiseleva and V. Brabec, *Eur. J. Biochem.*, 1995, **228**, 616–624.

23 M. Galanski and B. K. Keppler, *Anti-Cancer Agents Med. Chem.*, 2007, **7**, 55–73.

24 W. H. Ang, S. Pilet, R. Scopelliti, F. Bussy, L. Juillerat-Jeanneret and P. J. Dyson, *J. Med. Chem.*, 2005, **48**, 8060–8069.

25 M. D. Hall, H. R. Mellor, R. Callaghan and T. W. Hambley, *J. Med. Chem.*, 2007, **50**, 3403–3411.

26 T. C. Johnstone, K. Suntharalingam and S. J. Lippard, *Chem. Rev.*, 2016, **116**, 3436–3486.

27 V. Pichler, P. Heffeter, S. M. Valiahdi, C. R. Kowol, A. Egger, W. Berger, M. A. Jakupec, M. Galanski and B. K. Keppler, *J. Med. Chem.*, 2012, **55**, 11052–11061.

28 H. S. Oberoi, N. V. Nukolova, A. V. Kabanov and T. K. Bronich, *Adv. Drug Delivery Rev.*, 2013, **65**, 1667–1685.

29 X. Han, J. Sun, Y. Wang and Z. He, *Med. Res. Rev.*, 2015, **35**, 1268–1299.

30 G. Apps Michael, H. Y. Choi Eugene and J. Wheate Nial, *Endocr.-Relat. Cancer*, 2015, **22**, R219–R233.

31 S. Choi, C. Filotto, M. Bisanzo, S. Delaney, D. Lagasee, J. L. Whitworth, A. Jusko, C. Li, N. A. Wood, J. Willingham, A. Schwenker and K. Spaulding, *Inorg. Chem.*, 1998, **37**, 2500–2504.

32 S. Karmakar, K. Purkait, S. Chatterjee and A. Mukherjee, *Dalton Trans.*, 2016, **45**, 3599–3615.

33 B. A. Chabner and T. G. Roberts, *Nat. Rev. Cancer*, 2005, **5**, 65–72.

34 S. R. Rajski and R. M. Williams, *Chem. Rev.*, 1998, **98**, 2723–2795.

35 D. M. Noll, A. M. Noronha, C. J. Wilds and P. S. Miller, *Front. Biosci.*, 2004, **9**, 421–437.

36 D. C. Ware, P. J. Brothers, G. R. Clark, W. A. Denny, B. D. Palmer and W. R. Wilson, *Dalton Trans.*, 2000, 925–932.

37 D. C. Ware, W. A. Denny and G. R. Clark, *Acta Crystallogr., Sect. C: Cryst. Struct. Commun.*, 1997, **C53**, 1058–1059.

38 D. C. Ware, B. D. Palmer, W. R. Wilson and W. A. Denny, *J. Med. Chem.*, 1993, **36**, 1839–1846.

39 D. C. Ware, H. R. Palmer, F. B. Bruijn, R. F. Anderson, P. J. Brothers, W. A. Denny and W. R. Wilson, *Anti-Cancer Drug Des.*, 1998, **13**, 81–103.

40 D. C. Ware, B. G. Siim, K. G. Robinson, W. A. Denny, P. J. Brothers and G. R. Clark, *Inorg. Chem.*, 1991, **30**, 3750–3757.

41 D. C. Ware, W. R. Wilson, W. A. Denny and C. E. F. Richard, *J. Chem. Soc., Chem. Commun.*, 1991, 1171–1173, DOI: 10.1039/c39910001171.

42 P. R. Craig, P. J. Brothers, G. R. Clark, W. R. Wilson, W. A. Denny and D. C. Ware, *Dalton Trans.*, 2004, 611–618, DOI: 10.1039/b311091e.

43 B. A. Teicher, M. J. Abrams, K. W. Rosbe and T. S. Herman, *Cancer Res.*, 1990, **50**, 6971–6975.

44 S. V. Yakovlev, O. M. Nozdrina and V. B. Ukraintsev, *Zh. Obshch. Khim.*, 1992, **62**, 967–971.

45 S. V. Yakovlev, V. B. Ukraintsev, O. M. Nozdrina and Y. N. Kukushkin, *Zh. Obshch. Khim.*, 1990, **60**, 1321–1325.

46 J. J. Wilson and S. J. Lippard, *Chem. Rev.*, 2014, **114**, 4470–4495.

47 V. Y. Kukushkin, S. V. Yakovlev and V. B. Ukraintsev, *Koord. Khim.*, 1988, **14**, 969–971.

48 G. Schmid and G. Ritter, *Z. Anorg. Allg. Chem.*, 1975, **415**, 97–103.

49 J. Barry, J. G. H. Du Preez, E. Els, H. E. Rohwer and P. J. Wright, *Inorg. Chim. Acta*, 1981, **53**, L17–L18.

50 H. Schmidbaur and P. Jandik, *Inorg. Chim. Acta*, 1983, **74**, 97–99.

51 W. H. Beattie, W. B. Maier II and R. F. Holland, *J. Inorg. Nucl. Chem.*, 1978, **40**, 1885–1887.

52 F. Bottomley, J. Darkwa, L. Sutin and P. S. White, *Organometallics*, 1986, **5**, 2165–2171.

53 H. G. Alt, T. Frister, E. E. Trapl and H. E. Engelhardt, *J. Organomet. Chem.*, 1989, **362**, 125–134.

54 J. A. Broomhead, *J. Am. Chem. Soc.*, 1968, **90**, 4480–4482.

55 F. S. Mackay, J. A. Woods, P. Heringova, J. Kasparkova, A. M. Pizarro, S. A. Moggach, S. Parsons, V. Brabec and P. J. Sadler, *Proc. Natl. Acad. Sci. U. S. A.*, 2007, **104**, 20743–20748.

56 F. S. Mackay, S. A. Moggach, A. Collins, S. Parsons and P. J. Sadler, *Inorg. Chim. Acta*, 2009, **362**, 811–819.

57 L. Cubo, T. W. Hambley, P. J. Sanz Miguel, A. Carnero, C. Navarro-Ranninger and A. G. Quiroga, *Dalton Trans.*, 2011, **40**, 344–347.

58 J. Reedijk, *Chem. Commun.*, 1996, 801–806, DOI: 10.1039/cc9960000801.

59 R. M. Roat and J. Reedijk, *J. Inorg. Biochem.*, 1993, **52**, 263–274.

60 E. G. Talman, Y. Kidani, L. Mohrmann and J. Reedijk, *Inorg. Chim. Acta*, 1998, **283**, 251–255.

61 J. Lorberth, M. El-Essawi, W. Massa and L. Labib, *Angew. Chem., Int. Ed. Engl.*, 1988, **100**, 1194–1195.

62 U. Warnke, C. Rappel, H. Meier, C. Kloft, M. Galanski, C. G. Hartinger, B. K. Keppler and U. Jaehde, *ChemBioChem*, 2004, **5**, 1543–1549.

63 M. A. Medrano, A. Alvarez-Valdes, J. Perles, J. Lloret-Fillol, S. Munoz-Galvan, A. Carnero, C. Navarro-Ranninger and A. G. Quiroga, *Chem. Commun.*, 2013, **49**, 4806–4808.

64 J. Reedijk, *Chem. Rev.*, 1999, **99**, 2499–2510.

65 M. A. Fuertes, C. Alonso and J. M. Perez, *Chem. Rev.*, 2003, **103**, 645–662.

66 G. R. Gibbons, S. Wyrick and S. G. Chaney, *Cancer Res.*, 1989, **49**, 1402–1407.

67 A. Eastman, *Biochem. Pharmacol.*, 1987, **36**, 4177–4178.

68 Y. Kido, A. R. Khokhar and Z. H. Siddik, *Biochem. Pharmacol.*, 1994, **47**, 1635–1642.

69 A. Levina, A. Mitra and P. A. Lay, *Metallomics*, 2009, **1**, 458–470.

70 R. Trondl, P. Heffeter, C. R. Kowol, M. A. Jakupec, W. Berger and B. K. Keppler, *Chem. Sci.*, 2014, **5**, 2925–2932.

71 S. J. Berners-Price and P. W. Kuchel, *J. Inorg. Biochem.*, 1990, **38**, 305–326.

72 N. Barnes, M. Y. Bartee, L. Braiterman, A. Gupta, V. Ustiyan, V. Zuzel, J. H. Kaplan, A. L. Hubbard and S. Lutsenko, *Traffic*, 2009, **10**, 767–779.

73 M. Komatsu, T. Sumizawa, M. Mutoh, Z.-S. Chen, K. Terada, T. Furukawa, X.-L. Yang, H. Gao, N. Miura, T. Sugiyama and S.-I. Akiyama, *Cancer Res.*, 2000, **60**, 1312–1316.

74 G. Samimi, R. Safaei, K. Katano, A. K. Holzer, M. Rochdi, M. Tomioka, M. Goodman and S. B. Howell, *Clin. Cancer Res.*, 2004, **10**, 4661–4669.

75 N. V. Dolgova, D. Olson, S. Lutsenko and O. Y. Dmitriev, *Biochem. J.*, 2009, **419**, 51–56.

76 O. Y. Dmitriev, *Biochem. Cell Biol.*, 2011, **89**, 138–147.

77 V. Calandrini, F. Arnesano, A. Galliani, T. H. Nguyen, E. Ippoliti, P. Carloni and G. Natile, *Dalton Trans.*, 2014, **43**, 12085–12094.

78 Z. Liu, A. Habtemariam, A. M. Pizarro, S. A. Fletcher, A. Kisova, O. Vrana, L. Salassa, P. C. A. Bruijnincx, G. J. Clarkson, V. Brabec and P. J. Sadler, *J. Med. Chem.*, 2011, **54**, 3011–3026.

79 A. H. Wyllie, J. F. Kerr and A. R. Currie, *Int. Rev. Cytol.*, 1980, **68**, 251–306.

80 M. J. Arends, R. G. Morris and A. H. Wyllie, *Am. J. Pathol.*, 1990, **136**, 593–608.

81 A. H. Wyllie, *Nature*, 1980, **284**, 555–556.

82 M. Enari, H. Sakahira, H. Yokoyama, K. Okawa, A. Iwamatsu and S. Nagata, *Nature*, 1998, **391**, 43–50.

83 P. T. Daniel, I. Sturm, S. Ritschel, K. Friedrich, B. Dorken, P. Bendzko and T. Hillebrand, *Anal. Biochem.*, 1999, **266**, 110–115.

84 S. Nagata, *Cell*, 1997, **88**, 355–365.

85 D. R. Green and J. C. Reed, *Science*, 1998, **281**, 1309–1312.

86 D. R. Green and G. Kroemer, *Science*, 2004, **305**, 626–629.

87 G. Kroemer and J. C. Reed, *Nat. Med.*, 2000, **6**, 513–519.

88 S. T. Smiley, M. Reers, C. Mottola-Hartshorn, M. Lin, A. Chen, T. W. Smith, G. D. Steele Jr. and L. B. Chen, *Proc. Natl. Acad. Sci. U. S. A.*, 1991, **88**, 3671–3675.

89 E. A. Slee, M. T. Harte, R. M. Kluck, B. B. Wolf, C. A. Casiano, D. D. Newmeyer, H.-G. Wang, J. C. Reed, D. W. Nicholson, E. S. Alnemri, D. R. Green and S. J. Martin, *J. Cell Biol.*, 1999, **144**, 281–292.

90 M. O. Hengartner, *Nature*, 2000, **407**, 770–776.

91 N. A. Thornberry, T. A. Rano, E. P. Peterson, D. M. Rasper, T. Timkey, M. Garcia-Calvo, V. M. Houtzager, P. A. Nordstrom, S. Roy, J. P. Vaillancourt, K. T. Chapman and D. W. Nicholson, *J. Biol. Chem.*, 1997, **272**, 17907–17911.

92 J. F. Kerr, A. H. Wyllie and A. R. Currie, *Br. J. Cancer*, 1972, **26**, 239–257.

93 C. M. Seynaeve, M. Stetler-Stevenson, S. Sebers, G. Kaur, E. A. Sausville and P. J. Worland, *Cancer Res.*, 1993, **53**, 2081–2086.

94 P. Friedl and K. Wolf, *Nat. Rev. Cancer*, 2003, **3**, 362–374.

95 B. Naeye, H. Deschout, M. Roding, M. Rudemo, J. Delanghe, K. Devreese, J. Demeester, K. Braeckmans, S. C. De Smedt and K. Raemdonck, *Biomaterials*, 2011, **32**, 9120–9127.

96 H.-W. An, S.-L. Qiao, C.-Y. Hou, Y.-X. Lin, L.-L. Li, H.-Y. Xie, Y. Wang, L. Wang and H. Wang, *Chem. Commun.*, 2015, **51**, 13488–13491.

97 T.-Y. Liu, W. M. Hussein, A. K. Giddam, Z. Jia, J. M. Reiman, M. Zaman, N. A. J. McMillan, M. F. Good, M. J. Monteiro, I. Toth and M. Skwarczynski, *J. Med. Chem.*, 2015, **58**, 888–896.

98 A. Sarkar, S. Bhattacharyya, S. K. Dey, S. Karmakar and A. Mukherjee, *New J. Chem.*, 2014, **38**, 817–826.